RSC Advances

ROYAL SOCIETY OF CHEMISTRY

www.rsc.org/advances

Nanodiamond-TiO_2 composites for photocatalytic degradation of microcystin-LA in aqueous solutions under simulated solar light

Maria J. Sampaio[1], Luisa M. Pastrana-Martínez[1], Adrián M.T. Silva[1,*], Josephus G. Buijnsters[2], Changseok Han[3], Cláudia G. Silva[1], Sónia A.C. Carabineiro[1], Dionysios D. Dionysiou[3,*], Joaquim L. Faria[1]

[1]LCM – Laboratory of Catalysis and Materials – Associate Laboratory LSRE-LCM, Faculdade de Engenharia, Universidade do Porto, Rua Dr. Roberto Frias s/n, 4200-465 Porto, Portugal

[2]Department of Precision and Microsystems Engineering, Research Group of Micro and Nano Engineering, Delft University of Technology, Mekelweg 2, 2628 CD, Delft, The Netherlands

[3]Environmental Engineering and Science Program, University of Cincinnati, Cincinnati, OH 45221, United States

*Corresponding authors:

adrian@fe.up.pt (A.M.T. Silva); dionysios.d.dionysiou@uc.edu (D.D. Dionysiou)

Abstract

Titanium dioxide (TiO_2) has been under intensive investigation for photocatalytic degradation of cyanobacterial toxins. In order to develop more efficient photocatalysts, TiO_2 and oxidized nanodiamonds (ND_{ox}) were combined as a composite catalyst (ND_{ox}–TiO_2), which was tested in the oxidation of microcystin-LA (MC-LA), a cyanotoxin frequently found in freshwaters. ND_{ox}–TiO_2 and neat TiO_2 photocatalysts were prepared by a liquid phase deposition method. A wide variety of analytical techniques, including physical adsorption of nitrogen, X-ray diffraction (XRD), UV-Vis and IR diffuse reflectance spectroscopies (DRUV-Vis and DRIFT), X-ray photoelectron spectroscopy (XPS), scanning electron microscopy (SEM) and transmission electron microscopy (TEM), were used to characterize the materials. The performance of the photocatalysts was studied under both simulated solar and visible light. Kinetic results show remarkable efficiency for the ND_{ox}–TiO_2 composite under simulated solar light irradiation with a synergistic factor of more than 15 relative to neat TiO_2, while negligible photocatalytic activity was observed for the degradation of MC-LA when ND_{ox}-TiO_2 was used under visible light illumination due to the wide band gap of the composite material. The photocatalytic efficiency of ND_{ox}–TiO_2 was ascribed to the good dispersion of both phases in the composite material, facilitating the possible electronic interaction at the heterojunction interface between ND_{ox} and TiO_2.

Keywords: titanium dioxide; nanodiamonds; photocatalysis; cyanotoxins; microcystin-LA.

Introduction

The number and complexity of new water contaminants derived from the rapid growth of population and industrial activities are rendering the conventional water and wastewater treatment processes rather ineffective. The development of novel clean treatment technologies compatible with the environment for water treatment has been a continuous increasing

worldwide concern. Efficient heterogeneous photocatalytic processes using titanium dioxide (TiO_2) have been amply confirmed in literature.[1-6] In addition, various studies reported that the application of carbon materials such as carbon nanotubes[7, 8] and graphene derivatives[9-11] may improve the photocatalytic activity of TiO_2 in water/wastewater treatment due to their unique specific properties and the possibility to control these properties by structural and compositional modification.

Recently, nanodiamonds (NDs) have been used as alternative carbon materials towards the development of efficient photocatalysts upon combination with TiO_2.[12] Diamonds (carbon with sp^3 hybridization) are potentially applicable candidates for composite synthesis due to their unique chemical, structural, mechanical, biological and optical properties.[13, 14] In fact, these materials are being increasingly used in a wide variety of applications (medicine, biotechnology, catalysis, among others). The cost of NDs is mostly dictated by the technique employed in their production. Nowadays, they are obtained on a large scale, by relatively inexpensive detonation processes of carbon-containing explosives.[15] NDs produced by detonation of carbon explosive materials are commonly defined as diamonds with small sizes (typically 4-5 nm) that have high specific surface areas (around 300 $m^2 g^{-1}$) allowing to create large amounts of reactive chemical surface groups.[16]

To the best of our knowledge, there is only one study[12] where some of us describe the application of NDs–TiO_2 composites for photocatalytic water treatment. In such report a significant improvement in the photocatalytic activity was observed for degradation of an organic pharmaceutical water pollutant (diphenhydramine) when NDs were combined with TiO_2, using an optimal content of oxidized NDs (i.e., 15 *wt.* % of ND_{ox}).

Microcystins (MCs), the most widespread cyanotoxins present in diverse aqueous environments, cause water quality problems for fisheries, aquaculture and sanitary hazard for human and animal.[17-19] The most common and studied MC found in freshwaters is the variant MC-LR, which has been widely employed as model cyanotoxin in photocatalysis.[20-22] Other

commonly detected variants in freshwaters include MC-YR, MC-RR and MC-LA,[23] which are less studied. In this regard, the present work is focused on the degradation of MC-LA (the microcystin most similar to MC-LR) in water under simulated solar light and employing a ND_{ox}–TiO_2 composite photocatalyst with 15 *wt.*% ND_{ox} content.

Experimental

Synthesis of photocatalysts

NDs (< 10 nm) were purchased from Sigma Aldrich and oxidized (ND_{ox}) by heating (at 703 K) in an open-air oven for several hours, as described elsewhere.[24, 25] A ND_{ox}–TiO_2 composite with 15 *wt.*% ND_{ox} loading was synthesized by a liquid phase deposition procedure (LPD)[12] as follows: oxidized NDs were dispersed in water under ultrasonication during 60 min and then the TiO_2 precursor $(NH_4)_2TiF_6$ (purity > 99.99%, Sigma Aldrich) and H_3BO_3 (purity > 99%, Fluka) in a molar ratio of 1:3 were added to the suspension. Then, the mixture was heated up to 333 K for 2 h under magnetic stirring. The obtained material was treated at 473 K under N_2 flow. The neat TiO_2 was prepared by the same procedure but without addition of ND_{ox} and applying the thermal treatment under the same conditions (N_2, 473 K).

Photocatalyst characterization

The N_2 adsorption-desorption isotherms at 77 K were obtained in a Quantachrome NOVA 4200e apparatus. The Brunauer, Emmett and Teller specific area (S_{BET}) was obtained from the N_2 adsorption data in the relative pressure range 0.05-0.20. The ND_{ox} content (*wt.*%) in ND_{ox}–TiO_2 was confirmed by thermogravimetric (TG) analysis by heating the sample in a flow of air from 323 up to 1273 K at 20 K min^{-1} using a STA 490 PC/4/H Luxx Netzsch thermal analyzer. X-ray diffraction (XRD) analysis was performed in a PANalytical X'Pert MPD equipped with an X'Celerator detector and secondary monochromator (Cu Kα λ = 0.154 nm, 50 kV, 40 mA; data recorded at a 0.017° step size, 100 s/step). Rietveld refinement with a PowderCell

software was applied for identification of the crystallographic phases and to calculate the crystallite size. The morphology of the materials was analyzed by scanning electron microscopy (SEM) using a Philips XL 30 ESEM-FEG apparatus. Transmission electron microscopy (TEM) was performed in a Philips CM20 equipment.

Diffuse reflectance infrared Fourier transform (DRIFT) spectroscopic analysis of the materials was performed on a Nicolet 510P FTIR Spectrometer, converting the interferograms to equivalent absorption units in the Kubelka–Munk scale. Diffuse reflectance UV–Vis spectra (DRUV-Vis) of the materials were measured on a JASCO V-560 UV-Vis spectrophotometer equipped with an integrating sphere. The spectra were recorded in diffuse reflectance mode and transformed to equivalent absorption Kubelka–Munk units. The band gap of the photocatalyst was determined using the Kubelka–Munk units as a function of the energy.

X-ray photoelectron spectroscopy (XPS) was performed in a Kratos AXIS Ultra HSA apparatus using a monochromatic Al Kα X-ray source (1486.7 eV), operating at 15 kV (90 W), in FAT mode (Fixed Analyser Transmission), with a pass energy of 40 eV for regions of interest and 80 eV for survey. Multi-region spectra were recorded at C 1s, O 1s and Ti 2p photoelectron peaks.

Photocatalytic experiments

The photocatalytic degradation of MC-LA 0.2 μM (99.3%, CalBiochem) was evaluated under natural pH conditions (pH = 5.7). The total volume of the MC-LA solution treated was 10 mL and the catalyst load was kept at 0.5 g L^{-1}. The experimental setup is described in detail elsewhere.[12] The irradiation source consisted in a xenon lamp (OF 300W 67005, Newport, Oriel Instrument) to simulate solar light irradiation (light irradiance of 47.1 mW cm^{-2}). For the experiments under visible light, two 15 W fluorescent lamps (Cole-Parmer) with a UV block filter (UV420, Opticology) were applied as irradiation source (irradiance of 0.4 mW cm^{-2}). The

photocatalytic experiments were performed in triplicate for each catalyst. Experiments in the absence of catalyst were also carried out to characterize the pure photochemical regime.

The concentration of MC-LA was evaluated by High Performance Liquid Chromatography (HPLC) using an Agilent 1100 Series apparatus equipped with a photodiode-array detector (PDA) set at 238 nm. The stationary phase consisted in a C_{18} Discovery HS (Supelco) column (150 mm × 2.1 mm, 5 μm particle size) working at 313 K with a flow rate of 0.2 mL min^{-1} and an injection volume of 50 μL. The method of analysis is described elsewhere.[12]

Results and Discussion

Photocatalyst characterization

The carbon content was determined by thermogravimetric analysis. The catalysts (TiO_2 and ND_{ox}–TiO_2) were submitted to a thermal treatment under air flow and the weight loss was monitored. The obtained results were in agreement with the nominal carbon content (*i.e.* 15 *wt*.%), which corresponds to the difference between the weight loss observed for the ND_{ox}–TiO_2 composite and that obtained for the neat TiO_2. The S_{BET} values found for TiO_2, ND_{ox} and ND_{ox}–TiO_2 were 118, 253, and 81 m^2 g^{-1},[12] respectively. The S_{BET} of the ND_{ox}–TiO_2 composite (81 m^2 g^{-1}) was lower than the nominal value (138 m^2 g^{-1}) obtained by the weighted average of the S_{BET} of ND_{ox} and TiO_2 phases in the composite material (i.e., taking into account their relative weight contents), evidencing the contact between the surface of both phases or the formation of larger TiO_2 particles when the composite is prepared.

The X-ray powder diffractograms of TiO_2, ND_{ox} and ND_{ox}–TiO_2 composite are shown in Figure 1. The presence of crystalline anatase TiO_2 is confirmed by XRD measurements, where the peaks at 25.1º and 47.6º correspond to the lattice plane of (101) and (004), respectively. The anatase crystallite size, determined by Rietveld refinement from the XRD data is around 8 nm. The XRD analysis of ND_{ox} shows two signals at 44.0º and 75.3º, resulting from the diamond reflection (111) and (220) planes, respectively.[26] The crystallite dimension found for

ND_{ox} was 5 nm. The diffractogram of ND_{ox}–TiO_2 composite was similar to that obtained in the case of TiO_2 (Figure 1) with a small contribution of (111) reflection of ND_{ox}. No significant change on the crystallite size of ND_{ox} was observed for ND_{ox}–TiO_2 composite. Nevertheless, the crystallite dimension of TiO_2 slightly increases to 11 nm, which could be related with the lower S_{BET} of the composite in comparison with the respective nominal value. This increase in the crystallite TiO_2 dimensions has been previously reported for oxidized carbon nanotube-TiO_2 composites, being attributed to the competition of the TiO_2 precursor species to the oxidized sites at the surface of the carbon material during the synthesis process, affecting the size of the TiO_2 crystallites.[27]

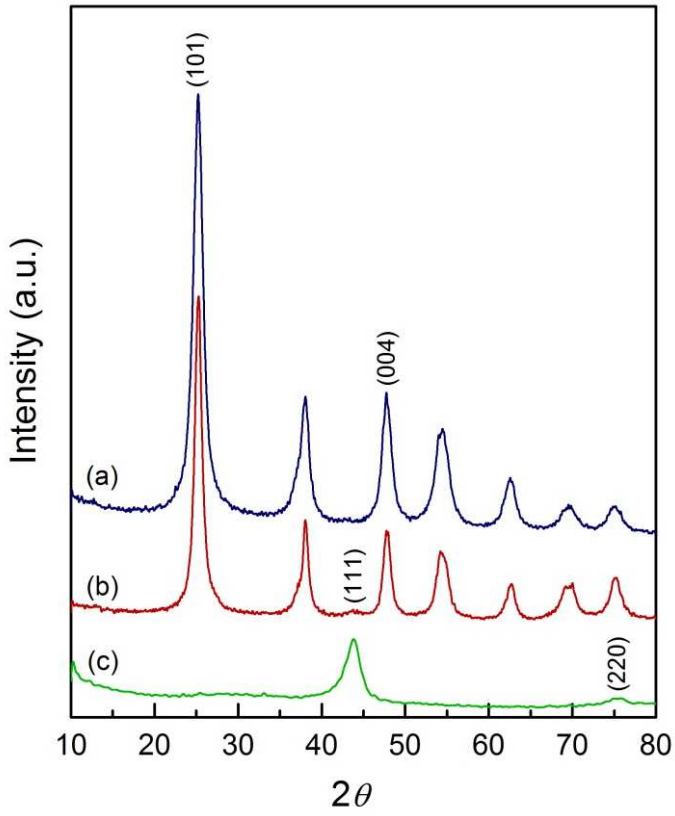

Figure 1. XRD diffractograms of (a) TiO_2, (b) ND_{ox}–TiO_2 and (c) ND_{ox} materials.

DRIFT analysis was performed for investigating possible interactions between TiO_2 and ND_{ox}, and the results are depicted in Figure 2. The DRIFT spectrum recorded for TiO_2 shows a broad band located between 2500 and 3800 cm^{-1} ascribed to the stretching vibrations of hydrogen-

bonded surface water molecules and hydroxyl groups. These observations are confirmed by the presence of a weak band centered at 1640 cm^{-1} associated to the bending vibration of water molecules as well as the presence of Ti-OH bonds.[28, 29] A typical band of TiO_2 materials around 970 cm^{-1} due to the Ti-O vibration was also observed,[28] while the sharp peak at 1420 cm^{-1} can be assigned to the lattice vibrations of TiO_2.[30, 31]

The DRIFT spectrum of ND_{ox} shows characteristic bands of surface oxidized carbon materials, with a broad band around 3400 cm^{-1} that can be usually attributed to vibration of C-OH groups of carboxylic acids and phenols, and to adsorbed water as confirmed by the presence of a OH bending mode at 1640 cm^{-1}. A small shoulder at c.a. 3000 cm^{-1} attributed to C-H stretching is also observed. The band at 1800 cm^{-1} can be assigned to the vibration of C=O bonds in carboxylic acids, carboxylic anhydrides, quinones and lactones, while the band peaking at 1470 cm^{-1} corresponds to C=C aromatic bending.[25] The bands in the range 1000 to 1300 cm^{-1} are characteristic of C-O stretching vibrations from anhydrides and lactones. As expected, previously reported temperature programmed desorption (TPD) analysis of ND_{ox} revealed that carboxylic acid groups are not present at the surface of ND_{ox} since the oxidation treatment was carried out at a temperature (703 K) higher than the decomposition temperature of these functional groups (around 503–649K).[12, 22, 32] Therefore, carboxylic anhydrides, lactones, phenols and carbonyl/quinone are the main oxygen groups present on the surface of ND_{ox}.

Regarding the DRIFT spectrum of the ND_{ox}–TiO_2 composite, the broadening of the intense band centered at 970 cm^{-1} (characteristic of Ti-O) can be assigned to Ti-O-C bonds,[33] thus suggesting the creation of an heterojunction at the interface between ND_{ox} and TiO_2. The bands at c.a. 1640 and 1470 cm^{-1} became more intense in the spectrum of the composite, resulting from the additive contribution of the vibration bands observed for both TiO_2 and ND_{ox} phases. Yet, the ND_{ox} band at 1800 cm^{-1} corresponding to carbonyl group vibration practically disappeared, while the broad band at 3400 cm^{-1} became less intense, indicating the existence of an interphase interaction between ND_{ox} and TiO_2.

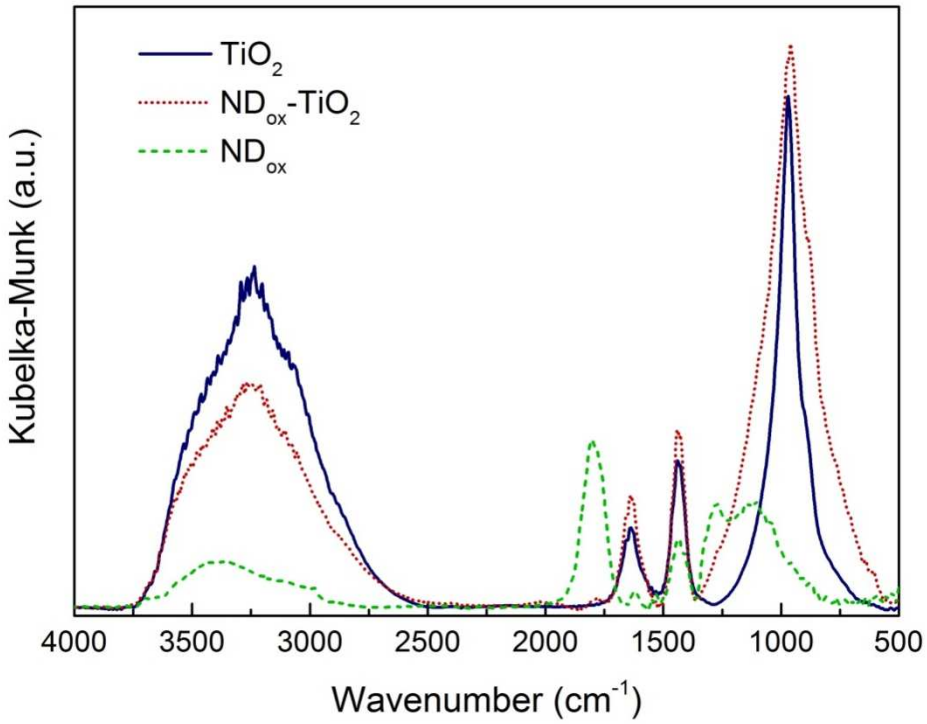

Figure 2. DRIFT spectra of ND_{ox}, TiO_2 and ND_{ox}–TiO_2 materials.

XPS deconvolution spectra of the of Ti 2p, C 1s and O 1s binding regions of TiO_2 and the ND_{ox}-TiO_2 composite were performed in order to identify possible chemical interactions between the elements in the near surface range. The XPS spectrum of Ti 2p region for ND_{ox}-TiO_2 (Figure 3a) shows two peaks at binding energies of 458.8 and 464.5 eV, corresponding respectively to Ti $2p_{3/2}$ and Ti $2p_{1/2}$ spin-orbital splitting photoelectrons (5.7 eV) in the Ti^{4+} chemical state,[34, 35] as also observed for neat TiO_2. In contrast, the spectra of O 1s core level for TiO_2 (Figure 3b) and ND_{ox}-TiO_2 (Figure 3c) were slightly different (insight of Figure 3c is shown for better comparison). While neat TiO_2 exhibits two peaks centered at 529.9 eV and 531.1 eV in the O 1s spectrum (Figure 3b), which are due to the lattice of Ti-O bond and –OH groups, respectively, the deconvolution fitting for the ND_{ox}-TiO_2 composite shows three constituents centered at 529.9, 531.1 and 532.7 eV (Figure 3c), that could be attributed to the presence of Ti-O, -OH and carbon phase (C-O) bonds, respectively.[4, 36] In the case of the C 1s core level spectra (not shown), carbon bonds were identified for neat TiO_2, probably resulting

from some organic species that were not removed by the thermal treatment (N_2, 473 K). Even so, it was possible to conclude that C-O (287.0 eV) [37, 38] is the main bond in the composite (as expected due to the known carbon sp^3 hybridization in diamonds), followed by C-C/C-H (285.0 eV) and C=O (288.9 eV),[37, 38] while other type of chemical bonds cannot be confirmed by this characterization technique. These results are in agreement with TPD analysis,[12] were phenol or ether (C-OH, C-O-C; 286.3 eV [36]) and quinone (C=O) groups were detected, while carboxylic acids (-COOH), carboxylic anhydrides (-$C(O)_2O$) and lactones (-COO) were not identified in the composite.

Several authors[39, 40] have reported that detonated NDs when dispersed in liquid medium induce strong particle aggregation, attributing the phenomenon to the harsh conditions in the detonation chamber that leads to the creation of dandling bonds on the ND surface. The free electron surfaces can cooperate via intermolecular surface forces such as van der Waals and hydrogen bonding creating covalent bonds between the primary particles.[39] This finding combined with the air oxidation treatment of NDs, which has been proved to increase the functional groups at the surface of NDs,[12] can promote the interphase interaction between ND_{ox} and TiO_2.

Figure 4 shows the DRUV-Vis spectra of the photocatalysts. A characteristic absorption sharp edge rising at 400 nm was observed for TiO_2. For this material, the valence band (VB) is composed of O 2p states and the conduction band (CB) is composed of Ti 3d states. The 330 nm absorption band is attributed to the charge transfer from O 2p to Ti 3d.[41] In case of the ND_{ox}–TiO_2 spectrum it was notice that the TiO_2 band is blue-shifted by the incorporation of ND_{ox} and a decrease in the shoulder tail in the UV range being also observed. These observations can be attributed to the creation of site defects at the TiO_2 crystalline structure, which can be linked with the carbon phase.

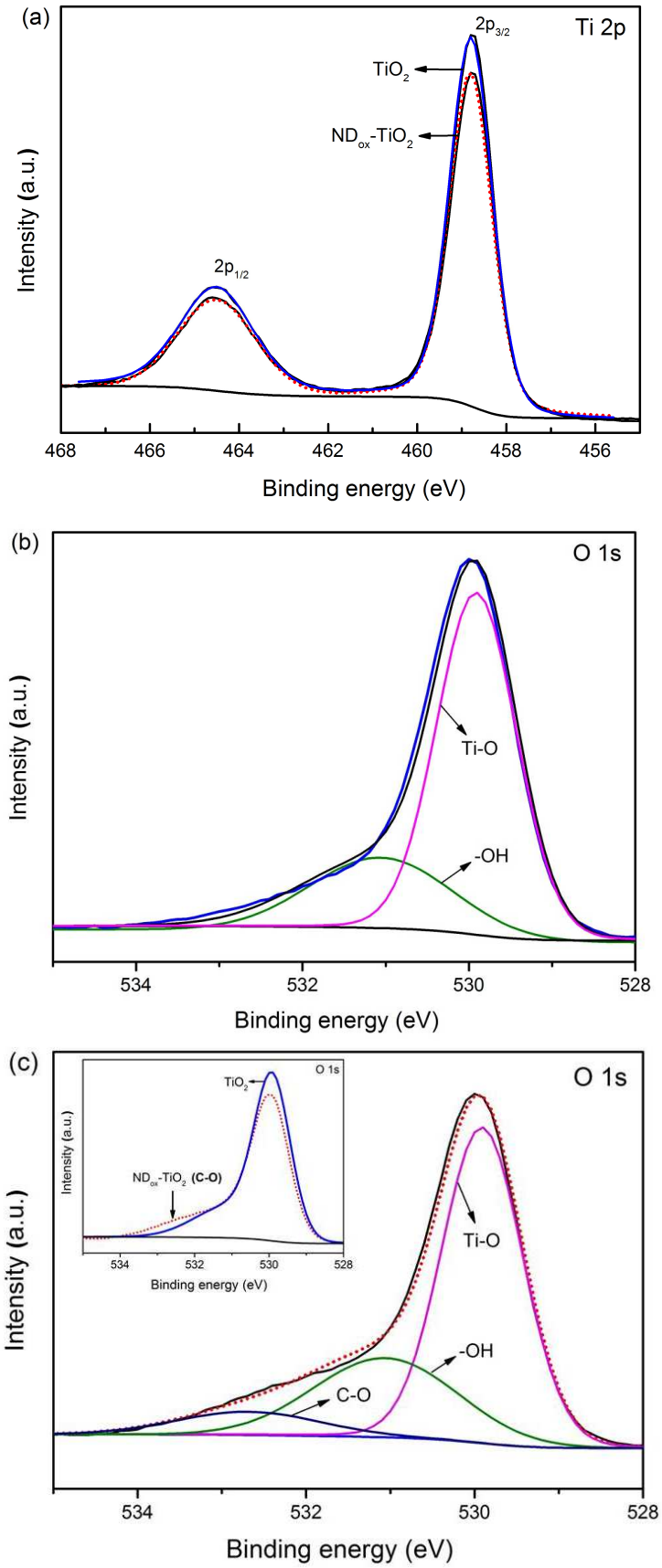

Figure 3. XPS peak deconvolution of the binding energy regions: (a) Ti 2p for TiO_2 and ND_{ox}-TiO_2, (b) O 1s for TiO_2, (c) O 1s for ND_{ox}-TiO_2 (inset: comparison of O 1s spectra).

The transformed Kubelka-Munk function was plotted as a function of the energy of light (Figure 4 inset) for the determination of the bandgap of the semiconductor materials. The band gaps for TiO_2 and ND_{ox}–TiO_2 were estimated as 3.26 and 3.41 eV, respectively. Quantum size and electronic interphase effects may constitute the major contributions for the increase of the bandgap energy of the composite material. Also, the high band gap of ND (5.0 eV [42, 43]) when mixed with TiO_2 may contribute to the increase of the band gap energy of the resulting composite material.

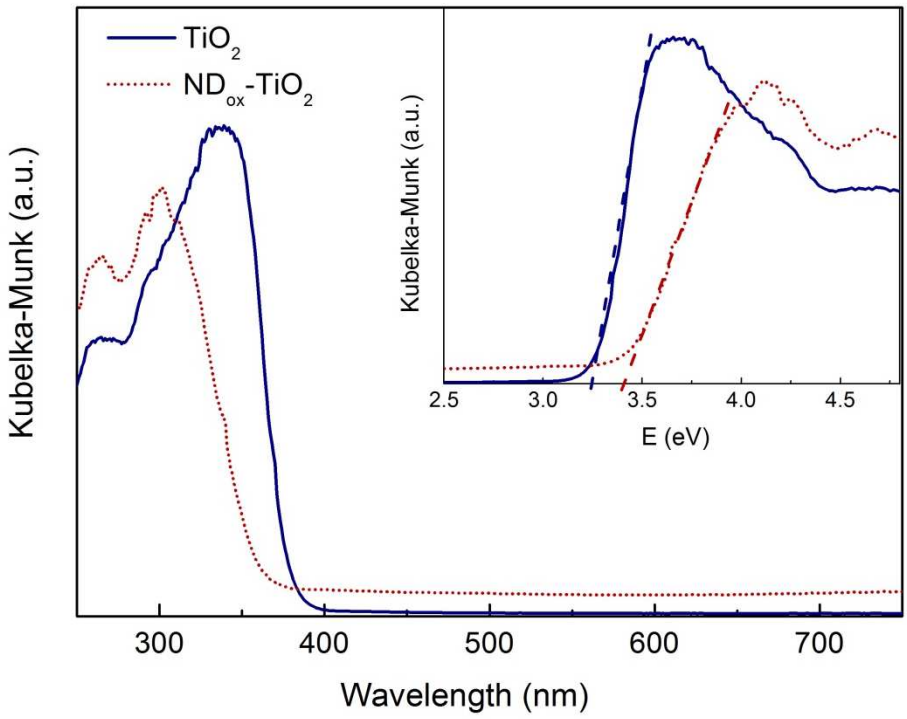

Figure 4. DRUV-Vis spectra of TiO_2 and ND_{ox}–TiO_2, and plot of Kubelka–Munk units as a function of the light energy (inset).

The representative SEM micrographs of TiO_2, ND_{ox}, and ND_{ox}–TiO_2 are shown in Figures 5a, 5c and 5e, respectively (higher magnifications are shown as insets). The structural morphology of neat TiO_2 (Figure 5a) significantly differs from the ND_{ox}–TiO_2 composite (Figure 5e). The neat TiO_2 presents spherical-like particles aggregated to form larger (micron-size) particles and consisting of small anatase crystallites as determined by XRD analysis. It is known that when

NDs are functionalized with oxygen-containing functional groups, the microscale morphology consists of small nanoparticles forming porous aggregates (as observed in Figure 5c) due to hydrogen bonding and van der Waals forces between the particles.[42] ND_{ox}-TiO_2 shows a convoluted morphology, where particles of very small dimensions are grouped forming composite clusters (Figure 5e).

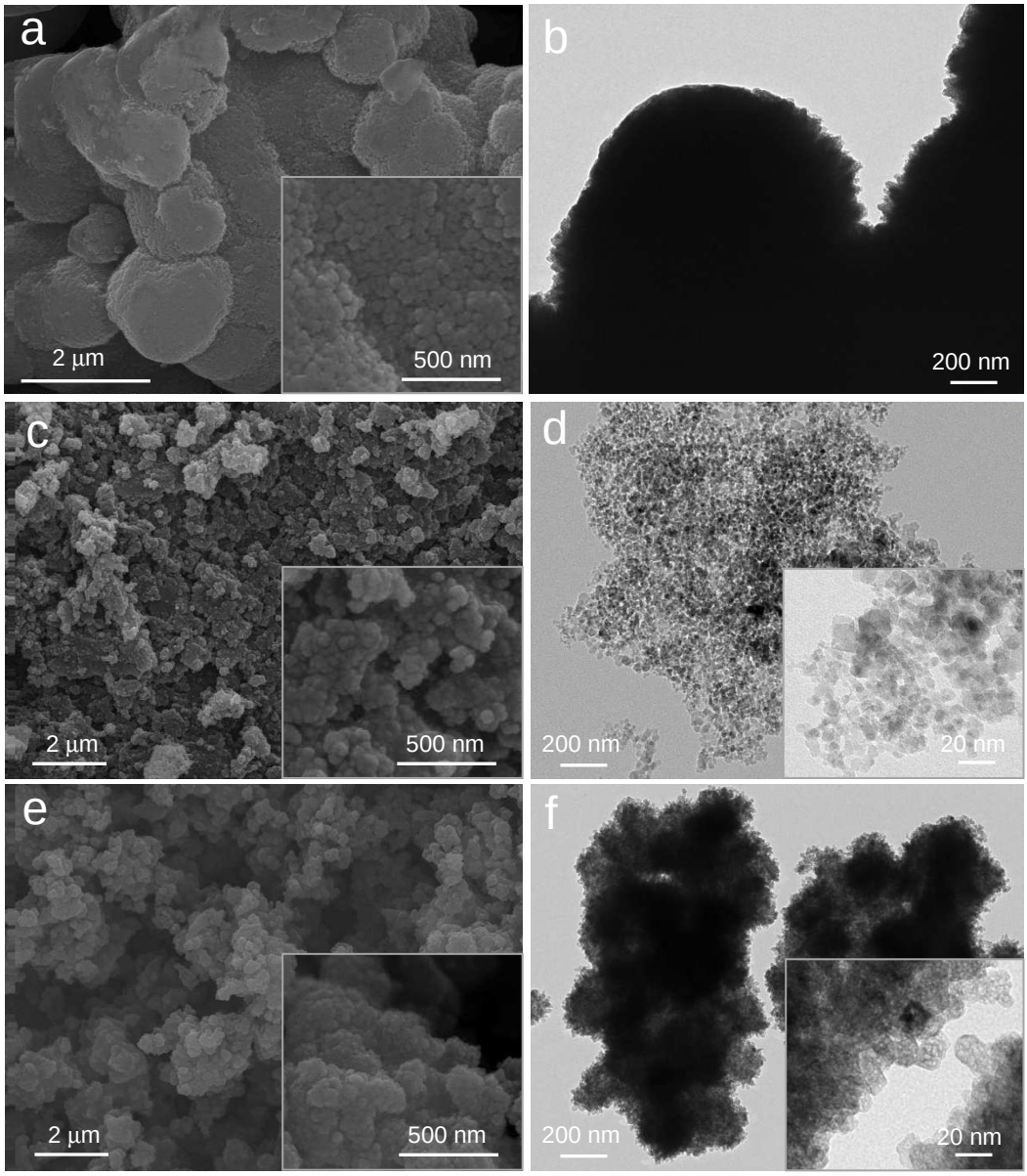

Figure 5. SEM (a, c, e) and TEM (b, d, f) images of neat TiO_2, ND_{ox}, and ND_{ox}–TiO_2, respectively.

TEM micrographs of TiO_2, ND_{ox} and ND_{ox}-TiO_2 are shown in Figures 5b, 5d and 5f, respectively. The micrograph of bare TiO_2 (Figure 5b) suggests that the already observed TiO_2 spherical particles are quite dense.[12] The TEM micrographs of ND_{ox} (Figure 5d) reveal that the aggregates are formed by small (~5 nm) nanoparticles of NDs confirming the value obtained by XRD analysis. The TEM micrograph of the ND_{ox}–TiO_2 composite reveals a homogeneous distribution of TiO_2 and ND_{ox} particles forming small clusters of okenite-like structures (Figure 5f).

Photocatalytic degradation of microcystin-LA

The photocatalytic activity of neat TiO_2, ND_{ox}, and ND_{ox}–TiO_2 materials was assessed in the degradation of MC-LA under simulated solar and visible light irradiation. A blank experiment was also performed, in the absence of any catalyst, for comparison purposes. No MC-LA degradation was observed by direct photolysis, confirming its resistance under such conditions, while the photocatalytic degradation of MC-LA under simulated solar light follows a pseudo-first order rate law (Figure 6a).

The apparent first order constants (k_{app}), determined by non-linear curve fitting to the experimental data, indicate that no appreciable MC-LA degradation when the pristine ND_{ox} sample was used (k_{app}= 9.8×10^{-4} min^{-1}), while the introduction of ND_{ox} to the TiO_2 matrix produced a notorious increase in the photocatalytic activity. In fact, ND_{ox}–TiO_2 (k_{app} = 4.4×10^{-1} min^{-1}) exhibits a k_{app} more than fifteen times larger than that for neat TiO_2 (k_{app} = 2.8×10^{-2} min^{-1}).

Superior surface area and narrow band gap are normally required attributes for enhanced efficiency of photocatalysts. However, these factors are not likely to be the main features contributing to the high efficiency observed for the ND_{ox}–TiO_2 composite when compared to the sole ND_{ox} and TiO_2 phases. Despite the high band gap of diamond, Nebel [44] inferred that this material could be a good candidate for photocatalytic applications due to its inert chemistry

and stability in liquids. The functional groups on the surface of air oxidized NDs, such as oxygen and hydroxyl species, can create a surface dipole layer that could affect their interfacial electron affinity. In other works, researchers even demonstrated that the presence of hydrogen bonds on H-terminated diamond surfaces could shift the conduction band above the vacuum energy level and the electrons can be directly transferred to the surrounding medium via surface states.[45, 46]

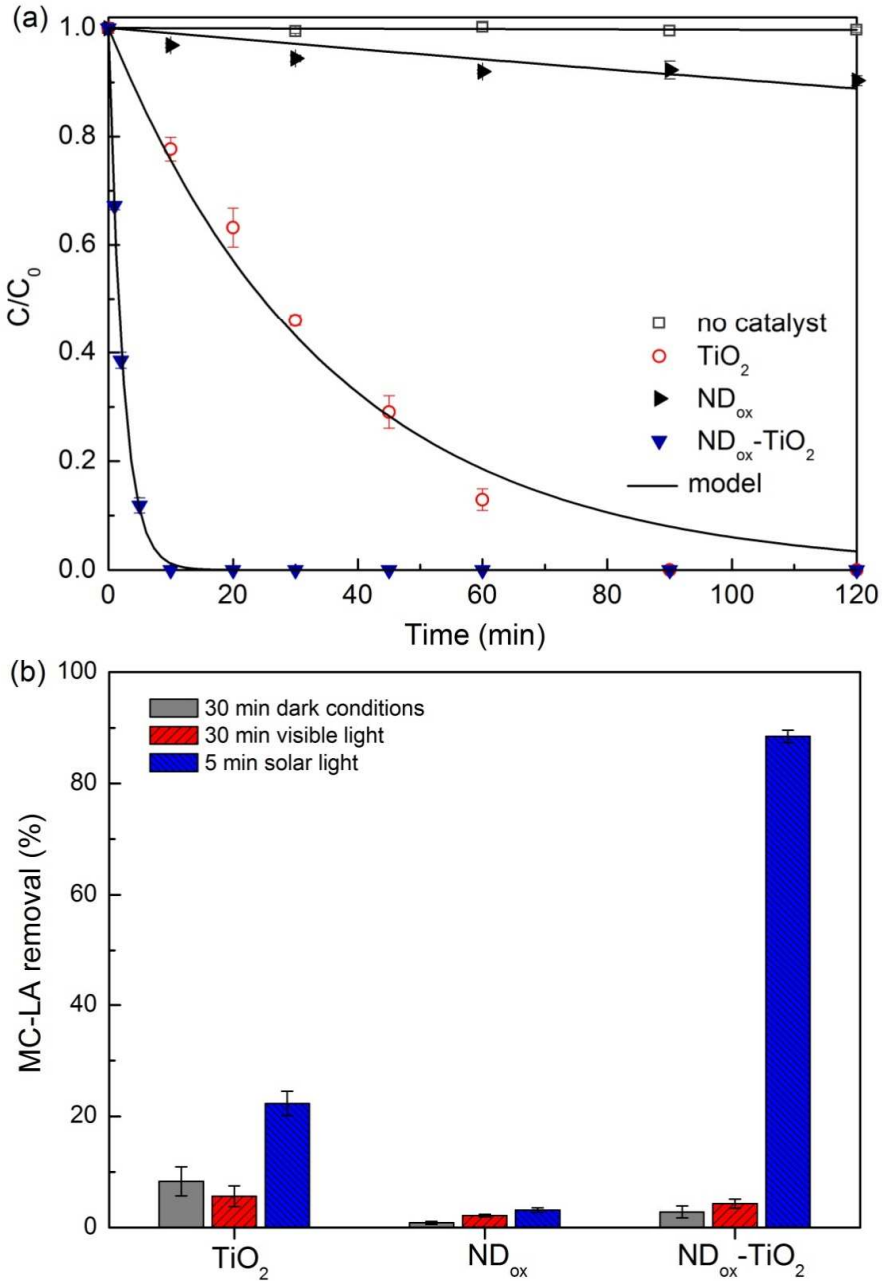

Figure 6. (a) Normalized concentration of MC-LA (C/C_0) using the different materials under simulated solar light. (b) MC-LA removal under dark conditions and both visible and solar light irradiation.

In view of above findings, the good dispersion of ND_{ox} and TiO_2 phases during the synthesis of the composite material can promotes the creation of strong electronic interphase interactions, as inferred from its characterization. Therefore, beneficial synergies and cooperative effects between the semiconductor and the carbon phase are expected, where electrons could be transferred from the ND_{ox} conduction band to the TiO_2 conduction band as well as the holes transferred from the TiO_2 valence band to the ND_{ox} valence band under light excitation. Thus, the separation of the photogenerated charges is facilitated, decreasing the occurrence of electron-hole recombination and leading to an increase of the ND_{ox}-TiO_2 photocatalytic activity.

Experiments under dark conditions were also performed to establish the adsorption equilibrium between MC-LA and the photocatalysts. As shown in Figure 6b, no significant adsorption was observed after 30 min, with a decrease of only 8%, 1% and 3% of the initial MC-LA concentration being observed using neat TiO_2, ND_{ox}, and ND_{ox}–TiO_2, respectively. In addition, it is important to refer that 30 min was proved to be sufficient to reach the adsorption equilibrium, as previously confirmed by performing dark adsorption runs for 5 h.

The results also show that the removal of MC-LA using TiO_2 or ND_{ox}–TiO_2 is negligible (Figure 6b) under visible light illumination (30 min), which is attributed to the large band gap energies of these materials[44] and thus low light absorption in the visible spectral range. No conversion was observed, even after 5 h of reaction (not shown), the apparent MC-LA removal being essentially related to adsorption. The wide band gap of NDs (~5 eV)[42-44] may also explain the inactiveness of ND_{ox} when irradiated at $\lambda > 400$ nm. TiO_2-based composites using other carbon materials, such as graphene oxide (GO-TiO_2) and carbon nanotubes (CNT-TiO_2),

have shown improved efficiency under simulated solar light and visible light radiation.[47, 48] A synergistic effect was found between the carbon and the TiO_2 phase, but low band gap energies were determined for these materials (2.95 eV and 3.04 eV, respectively). In particular, the lower band gap energy of GO-TiO_2 resulted in the best performance under visible light illumination. In contrast, negligible activity was observed when ND_{ox}-TiO_2 was tested under visible light due to the higher band gap of this composite (3.41 eV). Yet, improved efficiency was observed under solar irradiation (which includes UV-photoexcitation). Therefore, the low efficiency of ND_{ox}–TiO_2 under only visible illumination seems to be related with the optical properties of both TiO_2 and ND_{ox} materials. However, the ND_{ox}–TiO_2 composite shows to be highly efficient under real field conditions (i.e., solar light irradiation), of major relevance for solar applications. Thus, it will be now of interest to explore the combination of NDs with other TiO_2 materials presenting different crystalline phases and particle sizes.

Conclusions

ND_{ox}–TiO_2 composite and the respective bare materials (ND_{ox} and TiO_2) were synthesized, characterized and tested on the photocatalytic degradation of MC-LA in aqueous media under irradiation in the solar light and visible spectral range. The ND_{ox}–TiO_2 does not show any photocatalytic degradation of MC-LA under visible light, which can be explained by the wide band gap of the bare materials. However, the ND_{ox}–TiO_2 composite shows remarkably enhanced photocatalytic degradation of MC-LA under simulated solar light illumination with a synergistic factor of more than 15 relative to TiO_2, probably due to the good dispersion of both phases in the composite material and the creation of an electronic interphase interaction between the TiO_2 and ND_{ox} phases.

Acknowledgements

Financial support for this work was provided by project NORTE-07-0202-FEDER-038900 (NEPCAT) financed by FEDER (Fundo Europeu de Desenvolvimento Regional) through ON2 (Programa Operacional do Norte) and QREN, by project UID/EQU/50020/2013 financed by FCT(Fundação para a Ciência e a Tecnologia)/MEC and FEDER under Programe PT2020, and by projects NORTE-07-0162-FEDER-000050 and NORTE-07-0124-FEDER-000015 financed by QREN, ON2 and FEDER. MJS and LMPM acknowledge FCT for their research grants (SFRH/BD/79878/2011 and SFRH/BPD/88964/2012, respectively), while AMTS and SACC the FCT Investigator 2013 Programme (IF/01501/2013 and IF/1381/2013, respectively) with financing from the European Social Fund and the Human Potential Operational Programme. CH acknowledges the Graduate School Dean's Fellowship from the University of Cincinnati. The US National Science Foundation (US-Ireland collaborative research CBET (1033317)) and the Cyprus Research Promotion Foundation through Desmi 2009-2010 which is co-financed by the Republic of Cyprus and the European Regional Development Fund of the EU under contract number NEA IPODOMI/STRATH/0308/09 are also acknowledged.

References

1. C. G. Silva and J. L. Faria, *Journal of Photochemistry and Photobiology A: Chemistry*, 2003, **155**, 133-143.
2. A. Fujishima, T. N. Rao and D. A. Tryk, *Journal of Photochemistry and Photobiology C: Photochemistry Reviews*, 2000, **1**, 1-21.
3. M. Pelaez, N. T. Nolan, S. C. Pillai, M. K. Seery, P. Falaras, A. G. Kontos, P. S. M. Dunlop, J. W. J. Hamilton, J. A. Byrne, K. O'Shea, M. H. Entezari and D. D. Dionysiou, *Applied Catalysis B: Environmental*, 2012, **125**, 331-349.
4. H. Xu, S. Ouyang, L. Liu, P. Reunchan, N. Umezawa and J. Ye, *Journal of Materials Chemistry A*, 2014, **2**, 12642-12661.
5. L. Lin, Y. Yang, L. Men, X. Wang, D. He, Y. Chai, B. Zhao, S. Ghoshroy and Q. Tang, *Nanoscale*, 2013, **5**, 588-593.
6. L. Lin, Y. Chai, Y. Yang, X. Wang, D. He, Q. Tang and S. Ghoshroy, *International Journal of Hydrogen Energy*, 2013, **38**, 2634-2640.
7. R. Leary and A. Westwood, *Carbon*, 2011, **49**, 741-772.
8. B. Gao, G. Z. Chen and G. Li Puma, *Applied Catalysis B: Environmental*, 2009, **89**, 503-509.

9. S. Morales-Torres, L. M. Pastrana-Martínez, J. L. Figueiredo, J. L. Faria and A. M. T. Silva, *Environmental Science and Pollution Research*, 2012, **19**, 3676-3687.
10. Q. Xiang, J. Yu and M. Jaroniec, *Chemical Society Reviews*, 2012, **41**, 782-796.
11. D. Ravelli, D. Dondi, M. Fagnoni and A. Albini, *Chemical Society Reviews*, 2009, **38**, 1999-2011.
12. L. M. Pastrana-Martínez, S. Morales-Torres, S. A. C. Carabineiro, J. G. Buijnsters, J. L. Faria, J. L. Figueiredo and A. M. T. Silva, *ChemPlusChem*, 2013, **78**, 801-807.
13. A. M. Schrand, S. A. C. Hens and O. A. Shenderova, *Critical Reviews in Solid State and Materials Sciences*, 2009, **34**, 18-74.
14. O. A. Shenderova, V. V. Zhirnov and D. W. Brenner, *Critical Reviews in Solid State and Materials Sciences*, 2002, **27**, 227-356.
15. R. Kaur and I. Badea, *International Journal of Nanomedicine*, 2013, **8**, 203-220.
16. M. Ozawa, M. Inaguma, M. Takahashi, F. Kataoka, A. Krüger and E. Ōsawa, *Advanced Materials*, 2007, **19**, 1201-1206.
17. H. W. Paerl, N. S. Hall and E. S. Calandrino, *Science of The Total Environment*, 2011, **409**, 1739-1745.
18. J. H. Landsberg, *Reviews in Fisheries Science*, 2002, **10**, 113-390.
19. V. Gupta, S. K. Ratha, A. Sood, V. Chaudhary and R. Prasanna, *Algal Research*, 2013, **2**, 79-97.
20. M. Pelaez, A. A. de la Cruz, E. Stathatos, P. Falaras and D. D. Dionysiou, *Catalysis Today*, 2009, **144**, 19-25.
21. M. Antoniou, J. A. Shoemaker, A. A. de la Cruz and D. D. Dionysiou, *Toxicon*, 2008, **51**, 1103-1121.
22. J. L. Figueiredo, M. F. R. Pereira, M. M. A. Freitas and J. J. M. Órfão, *Carbon*, 1999, **37**, 1379-1389.
23. D. R. Figueiredo, U. M. Azeiteiro, S. M. Esteves, F. J. M. Gonçalves and M. J. Pereira, *Ecotoxicology and Environmental Safety*, 2004, **59**, 151-163.
24. S. Osswald, G. Yushin, V. Mochalin, S. O. Kucheyev and Y. Gogotsi, *Journal of the American Chemical Society*, 2006, **128**, 11635-11642.
25. O. Shenderova, A. M. Panich, S. Moseenkov, S. C. Hens, V. Kuznetsov and H. M. Vieth, *The Journal of Physical Chemistry C*, 2011, **115**, 19005-19011.
26. A. Nagata, T. Oku, K. Kikuchi, A. Suzuki, Y. Yamasaki and E. Osawa, *Progress in Natural Science: Materials International*, 2010, **20**, 38-43.
27. C. G. Silva and J. L. Faria, *Applied Catalysis B: Environmental*, 2010, **101**, 81-89.
28. C. G. Silva and J. L. Faria, *Photochemical and Photobiological Sciences*, 2009, **8**, 705-711.
29. S. Morales-Torres, L. M. Pastrana-Martínez, J. L. Figueiredo, J. L. Faria and A. M. T. Silva, *Applied Surface Science*, 2013, **275**, 361-368.
30. S. S. Mali, S. K. Desai, D. S. Dalavi, C. A. Betty, P. N. Bhosale and P. S. Patil, *Photochemical & Photobiological Sciences*, 2011, **10**, 1652-1660.
31. W. Yu-de, M. Chun-lai, S. Xiao-dan and L. Heng-de, *Journal of Non-Crystalline Solids*, 2003, **319**, 109-116.
32. W. H. Organization, *Journal*, 2014, **Volume 1: Coastal and fresh waters**.
33. G. Lui, J.-Y. Liao, A. Duan, Z. Zhang, M. Fowler and A. Yu, *Journal of Materials Chemistry A*, 2013, **1**, 12255-12262.
34. L. M. Pastrana-Martínez, S. Morales-Torres, V. Likodimos, J. L. Figueiredo, J. L. Faria, P. Falaras and A. M. T. Silva, *Applied Catalysis B: Environmental*, 2012, **123–124**, 241-256.
35. B. Erdem, R. A. Hunsicker, G. W. Simmons, E. D. Sudol, V. L. Dimonie and M. S. El-Aasser, *Langmuir*, 2001, **17**, 2664-2669.
36. C. H. Kim, B.-H. Kim and K. S. Yang, *Carbon*, 2012, **50**, 2472-2481.

37. Z. Zhao and Y. Dai, *Journal of Materials Chemistry A*, 2014, **2**, 13442-13451.
38. T. Kondo, I. Neitzel, V. N. Mochalin, J. Urai, M. Yuasa and Y. Gogotsi, *Journal of Applied Physics*, 2013, **113**, 214307.
39. R. Kaur and I. Badea, *International Journal of Nanomedicine*, 2013, **8**, 203–220.
40. M. Korobov, D. Volkov, N. Avramenko, L. Belyaeva, P. Semenyuk and M. Proskurnin, *Nanoscale*, 2013, **5(4)**, 36-1529.
41. B. Choudhury, M. Dey and A. Choudhury, *Int Nano Lett*, 2013, **3**, 1-8.
42. K. D. Behler, A. Stravato, V. Mochalin, G. Korneva, G. Yushin and Y. Gogotsi, *ACS Nano*, 2009, **3**, 363-369.
43. A. C. Ferrari and J. Robertson, *Physical Review B*, 2001, **63**, 121405(R).
44. C. E. Nebel, *Nat Mater*, 2013, **12**, 780-781.
45. D. M. Jang, Y. Myung, H. S. Im, Y. S. Seo, Y. J. Cho, C. W. Lee, J. Park, A.-Y. Jee and M. Lee, *Chemical Communications*, 2012, **48**, 696-698.
46. D. Zhu, L. Zhang, R. E. Ruther and R. J. Hamers, *Nature Materials*, 2013, **12**, 836-841.
47. L. M. Pastrana-Martínez, S. Morales-Torres, S. K. Papageorgiou, F. K. Katsaros, G. E. Romanos, J. L. Figueiredo, J. L. Faria, P. Falaras and A. M. T. Silva, *Applied Catalysis B: Environmental*, 2013, **142–143**, 101-111.
48. M. J. Sampaio, C. G. Silva, A. M. T. Silva, L. M. Pastrana-Martínez, C. Han, S. Morales-Torres, J. L. Figueiredo, D. D. Dionysiou and J. L. Faria, *Applied Catalysis B: Environmental*, 2015, **170–171**, 74-82.

Microcystin MC-LA degradation by a nanostructured solar photocatalyst

239x119mm (96 x 96 DPI)